Research on DC Bias Saturation Characteristics of Transformer Combining CEEMD and FuzzyEn Method

Xingmou Liu, Rui Lu, Ning Yang, Yao Xiao, Ammad Jadoon

***Abstract*—To address the challenge of accurately determining the saturation state induced by transformer DC bias, we propose a combined method for analyzing the DC bias of the transformer using vibration signals. This method employs the complementary ensemble empirical mode decomposition (CEEMD) to preprocess the vibration signals and fuzzy entropy (FuzzyEn) to assess the degree of DC bias. The optimal measurement point of the transformer is determined through transformer mechanical analysis. Subsequently, a vibration test. experimental platform is established to capture vibration signals at five distinct points on the transformer shell and core. These signals are then subjected to CEEMD for reconstruction, enabling the determination of the degree of DC bias. This assessment is based on fuzzy entropy values and difference curve analysis. The results demonstrate that the FuzzyEn value, serving as an indicator of the iron core's saturation due to DC bias, effectively detects the level of DC bias. Upon reaching its maximum value, the FuzzyEn of the vibration signal signifies the core's entry into the saturation zone. Specifically, the maximum FuzzyEn value is approximately 1.5 A on both sides of the core, about 1 A on the left and right sides of the shell, and 2 A in the middle of the shell. These findings confirm the efficacy of the combined CEEMD and FuzzyEn method.**

***Index Terms*—CEEMD reconstruction, Fuzzy Entropy, transformer vibration, DC bias**

I. Introduction

THE concept of the energy internet has been proposed and is poised for global development, driving the growing adoption of high voltage direct current (HVDC) transmission systems. These systems are favored for their ability to enhance power transmission capacity and ensure high stability over long-distance power delivery. However, when an HVDC transmission system is operated with a unipolar earth return line, the direct current flowing back from the ground can infiltrate the neutral grounded transformer windings, leading to DC bias magnetization of the transformer [1]. DC bias can induce saturation in the transformer core, pushing it beyond the linear operating range of magnetization. This leads to distortion in the excitation current and an upsurge in losses. Additionally, it can trigger issues such as abnormal transformer vibration and heightened noise levels [2].

The theoretical study of the DC bias problem involved a comprehensive analysis from both circuit and magnetic circuit perspectives [3], [4]. This analysis aimed to identify and propose potential modes arising from DC bias, offering insights into the various ways in which DC bias affects transformer performance. The proposal to describe the DC bias process through the DC magnetization curve offers a solution to the challenge of intuitively capturing the actual influence of DC under typical operating conditions [5]. This approach provides a more tangible representation, enhancing understanding and facilitating analysis of the magnetization process. The study focused on investigating the temperature rise of transformers operating under DC bias conditions [6]. By comparing transformer failure data with simulation results, the study determined the loss levels, temperature rise, and associated losses experienced by the transformer under DC bias conditions [7]. Primarily, the analysis aimed to understand the operational characteristics of transformers subjected to DC bias, providing insights into their performance and reliability under such conditions. The investigation delved into the phenomenon of transformer core saturation, identifying the magnetostrictive effect of the material as a crucial factor contributing to the vibration of transformer cores [8], [9], [10]. The experimental studies included vibration measurements to investigate the relationship between magnetostriction and vibration. These studies specifically accounted for transformer vibration, aiming to establish correlations between magnetostrictive effects within the transformer core and the resulting mechanical vibrations [11], [12]. In the aforementioned studies, transformer vibration was taken into consideration as a crucial aspect. The focus of the study is on conducting vibration analysis and extracting relevant features in the context of transformers operating under DC bias conditions. This research aims to comprehensively understand how DC bias affects transformer vibrations and to identify key

Manuscript received April 3, 2024; revised August 25, 2024.

This work was supported by the Science and Technology Research Program of Chongqing Municipal Education Commission (KJQN202200634) and the Ministry of Education Industry-University Cooperation Collaborative Education Program (220801480240051).

Xingmou Liu is a professor of Key Laboratory of Complex Systems and Bionic Control, Chongqing University of Posts and Telecommunications, Chongqing, 400000 China. (e-mail: liuxm@cqupt.edu.cn).

Rui Lu is a graduate student of Chongqing University of Posts and Telecommunications, Chongqing, 400065 China. (e-mail: 2535151279@qq.com).

Ning Yang is an engineer of State Grid Ningxia Electric Power Co. LTD Yinchuan Power Supply Company Yinchuan City, Ningxia, 750011 China. (corresponding author to provide phone: +08613883261469, e-mail: 791339327@qq.com).

Yao Xiao is an engineer of Chongqing Hongyu Precision Industry Group Co. LTD, Chongqing, China. (e-mail: 541294138@qq.com)

Ammad Jadoon is an assistant professor in the Department of Electrical Engineering at National University of Science and Technology, Islamabad, Pakistan. (e-mail: ammad.jadoon@nfciet.edu.pk).

characteristics or indicators associated with these vibrations [13], [14], [15]. The analysis focuses on understanding the vibration mechanism induced by DC bias in transformers and proposes a method for feature extraction to characterize this phenomenon. Subsequently, the proposed bias vibration features are validated by analyzing field data measurements obtained from transformers experiencing DC bias-induced vibrations. This comprehensive approach aims to provide deeper insight into the underlying mechanisms of DC bias-induced vibration in transformers and to establish reliable features for effective monitoring and diagnosis of transformer health under such conditions [16], [17]. Indeed, utilizing vibration methods for diagnosing transformer DC bias and assessing saturation state represents a relatively novel area with limited related studies. The complexity of transformer structures and components poses challenges in accurately selecting vibration test points, and assessing the degree of DC bias solely through iron core vibration measurements is inherently difficult. Given these complexities, a more objective approach involves analyzing vibrations from various parts of the transformer to monitor DC bias and determine saturation states. By examining vibrations across different components, a more comprehensive understanding of transformer behavior under DC bias conditions can be achieved, facilitating more accurate diagnosis and assessment of saturation states. This approach accounts for the multifaceted nature of transformer operation and provides a more holistic perspective on the effects of DC bias.

In this paper, we introduce a novel combined method employing complementary ensemble empirical mode decomposition (CEEMD) and fuzzy entropy (FuzzyEn) for analyzing transformer vibration signals under DC bias conditions [18]. CEEMD offers the advantage of decomposing vibration signals without imposing prior assumptions on the data, thereby enabling the division of the acquired signal into a series of intrinsic modal functions (IMFs) across different frequency bands and residuals [19]. Consequently, the CEEMD method is well-suited for effectively separating noisy modes. A key contribution of this work lies in the enhancement of transformer signals following CEEMD processing. The application of FuzzyEn for DC bias detection is proposed as a sophisticated method in addition to CEEMD. FuzzyEn offers the advantage of expressing the regularity of a time series across multiple dimensions and containing more time-dependent information [20]. This makes it particularly attractive for dynamic monitoring systems, where information about the temporal progression of defects is valuable not only for diagnosing the current machine condition but also for predicting its future behavior [21]. Thus, integrating FuzzyEn into the analysis enhances the capability to monitor transformer health and anticipate potential issues related to DC bias. The paper is structured as follows: First, a transformer mechanical analysis was performed to determine the optimal measurement point of the transformer [22]. Secondly, DC bias experiments are performed on a three-phase 5 kVA transformer to monitor the vibration signals at five different points on the core and casing. Finally, the principle and calculation process of CEEMD and FuzzyEn are presented. According to the transformer noise characteristics, the interference modes of the transformer vibration are filtered out by CEEMD reconstruction to obtain effective vibration signals. The harmonic characteristics of the vibration signal are analyzed using the reconstructed signal. The FuzzyEn values and differential curves of the reconstructed signal under DC bias are calculated.

II. Mechanical Analysis of Transformers

A. Transformer Physical Model

Analyze the mechanical properties of transformers in operation and perform computational studies on experimental transformers. The object of the study is a customized SG-5 transformer, the parameters of which are demonstrated in Table I. The transformer was modeled using COMSOL multiphysics field simulation software to obtain the solution domain and size (latent transformer enclosure) as shown in Fig. 1.

TABLE I
SG-5 TRANSFORMER PARAMETERS

Parameters	Numerical value
Nominal Voltage	400 V
No-Load Current	12 %
Short-Circuit Loss	160 W
Rated Capacity	5 kVA
No-Load Loss	75 W
Impedance Voltage	3.5 %

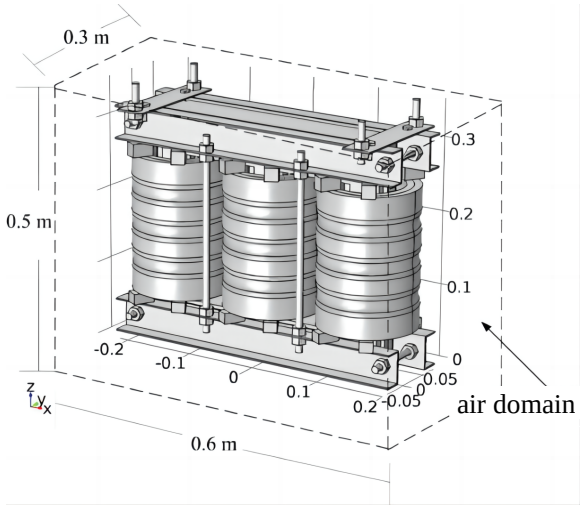

Fig. 1. The solution domain of the transformer

B. Model Solving and Calculations

The main purpose of the overall structural calculation of the transformer is to analyze the influence of the mechanical properties of each structural component through the transformer vibration source, which is a multi-physical field coupling problem of electricity-magnetism-force. A COMSOL secondary development interface and a hybrid programming method are used to numerically compute the electromagnetic and force fields of the transformer. This method uses the process iteration method of transient time, in which the physical fields are performed by successive sequences of convergent iterations within each point in time. Its computational flow is shown in Fig. 2.

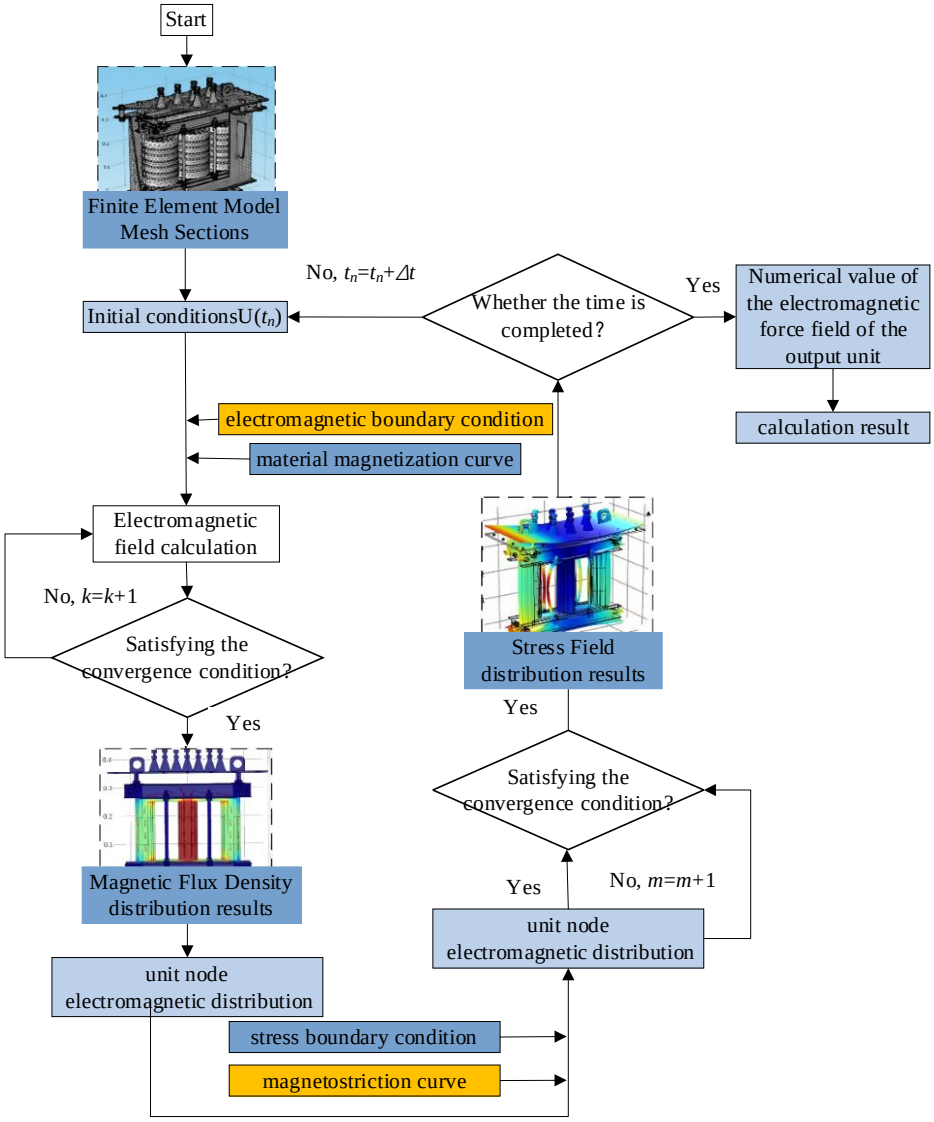

Fig. 2. Calculation flow chart of the transient model

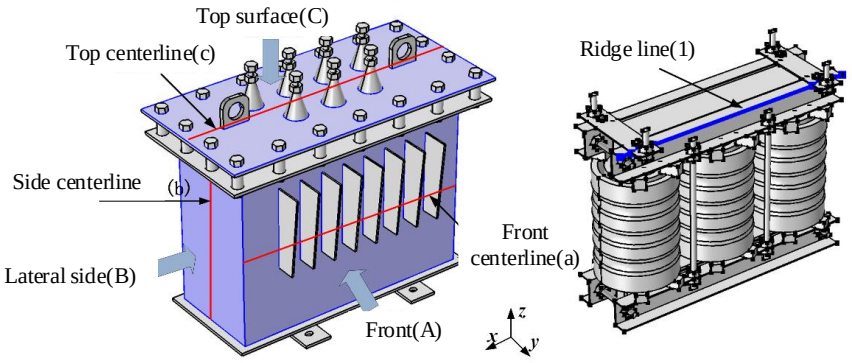

Fig. 3. Transformer structure and the analysis objects

A. Overall Structural Calculation and Analysis

The distribution of each field of transformer electric-magnetic-force can be derived by using COMSOL for multi-physical field coupling, and the results are analyzed. The focus is on the mechanical property characteristics of the transformer, therefore, the transformer structural parts and casing are selected as the objects of study when carrying out the research. As shown in Fig. 3, the three directional surfaces of the transformer casing are: front face A, side face B, and top face C. The axes on each surface are labeled as Line A, Line B, and Line C. The edge ridges of the structural member are called Line 1.

Mechanical properties analysis of internal structural parts: Selected the surface line of the clamped parts as the object of study. The deformation of the line along the x, y, and z axes was calculated separately, and the results are shown in Fig. 4. The results show that the ridge line on the surface of the structural part at a single power frequency exhibits a periodic change twice the power frequency. Simultaneously, the deformation distribution of the left and right parts is asymmetric, and this asymmetry does not change with time.

Fig. 4(a) demonstrates the deformation of the line in the x-direction. Upon observation, it can be found that the deformation directions of the left and right ends differ, with the left end dominated by the negative direction and the right end by the positive direction. Fig. 4(b) illustrates the deformation of the line in the y-direction. It is found that the y-direction deformation is mainly concentrated in the central region, and the magnitude of deformation varies drastically. The direction of deformation alternates between positive and negative directions, which is very pronounced. Fig. 4(c) shows the deformation of the line in the z-direction. It can be seen that both the left and right sides of the z-direction experience only positive deformation, and the amplitude changes are very drastic. In the center, the deformation alternates between positive and negative directions. This uniform deformation is primarily caused by the phase difference of the three-phase magnetic flux inside the transformer.

The mechanical analysis of the box shell focuses on investigating the behavior of the three surfaces of the shell. Fig. 5 shows the results of the deformation distribution of the transformer case at certain moments. Fig 5(a) indicates that the deformation of the front face is primarily concentrated in the middle under the influence of multiple forces. The maximum deformation gradually shifts to the leftover time and decreases uniformly, with the influence gradually dispersing in all directions. Fig. 5(b) illustrates the deformation distribution on the side face, where the degree of deformation varies gradually from bottom to top over time, showing a more even change. Fig. 5(c) demonstrates the deformation of the top surface over time, where the maximum value alternates between the left and right ends. Additionally, the outer edges of the top surface exhibit larger deformation magnitudes compared to the central portion.

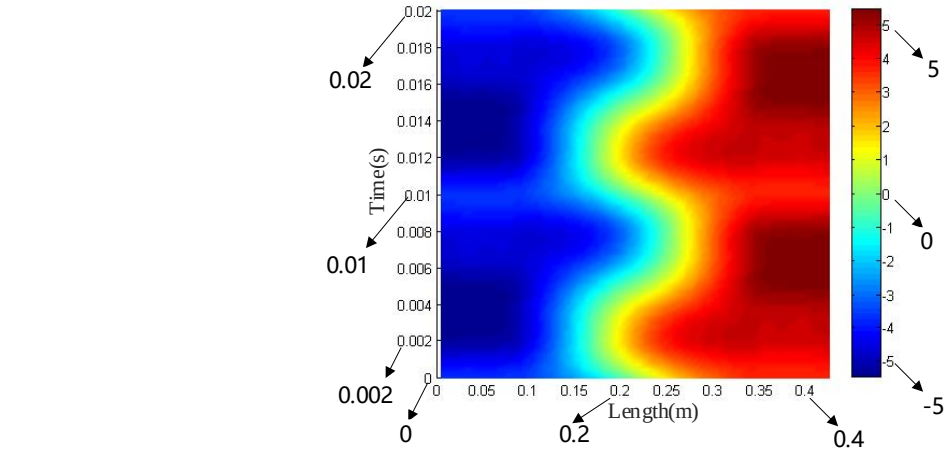

(a) x Direction

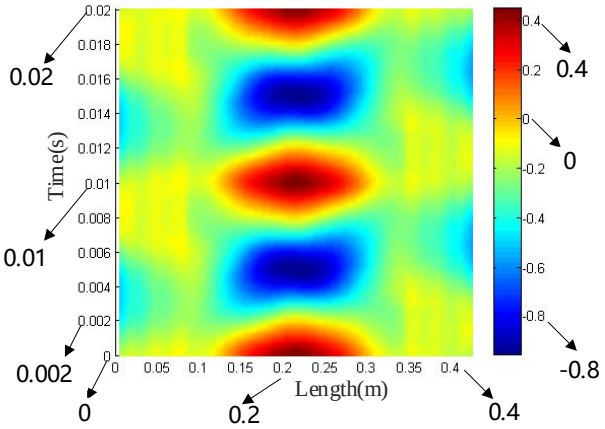

(b) y Direction

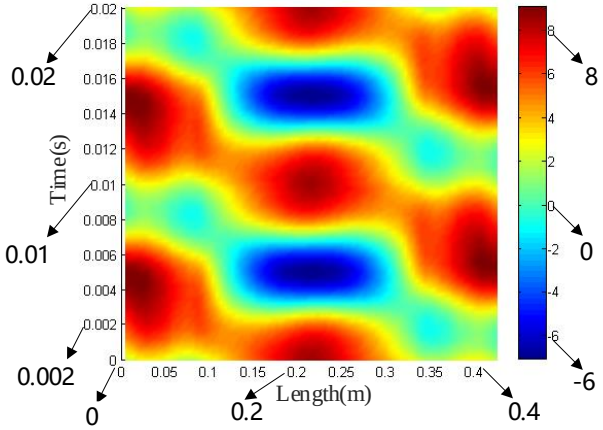

(c) z Direction

Fig. 4. The deformation change on the ridge

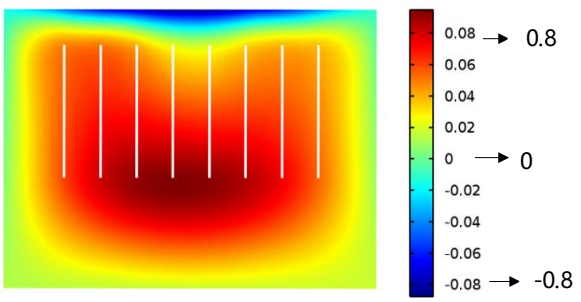

t=0.00175 s

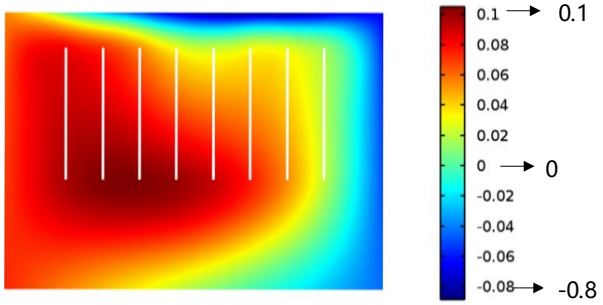

t=0.0065 s

(a) Front A

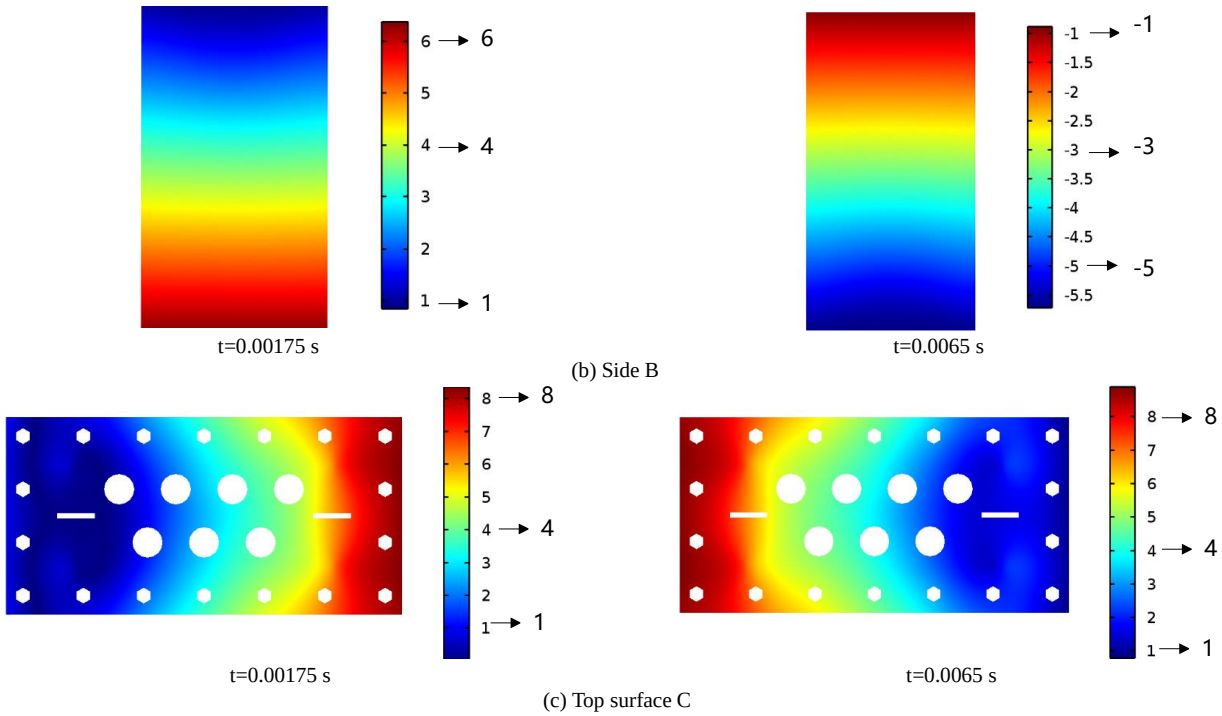

Fig. 5. Transformer shell surface deformation changes

I. Transformer DC Polarization Vibration Test

A. Vibration Test System Design

This paper analyzes the vibration of transformer cores through experimental methods. A vibration testing system is constructed to measure vibration signals at various points on both the transformer core and casing.

Sensors are employed to capture the vibration acceleration of the transformer core. During testing, a piezoelectric acceleration sensor is utilized, with its performance characteristics detailed in Table II. The experimental setup is illustrated in Fig. 6. The test procedure is depicted in Fig. 7.

TABLE II
IC PIEZOELECTRIC ACCELERATION SENSOR

Sensitivity	Range	Frequency	Resonant	Resolution
1000m V/g	5 g	0.1-2000 Hz	7.5 kHz	0.00002 g

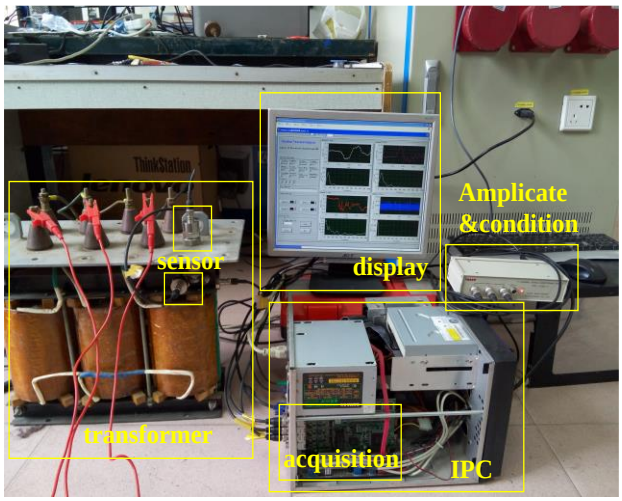

Fig.6. Experimental system of vibration test

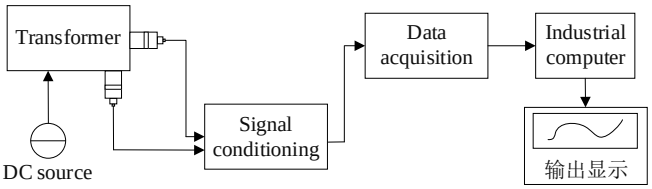

Fig.7. Block diagram of the test system

Vibration signals from the transformer are captured using vibration sensors, which are crucial for monitoring different operating states under both normal conditions and post-DC injection. These sensors typically operate based on acceleration or velocity measurement principles, converting mechanical vibrations from the transformer into electrical signals. Given the typically weak nature of vibration signals, amplification to an appropriate range is required using a signal amplifier. Additionally, because acquired signals may contain noise and interference, they are processed by a signal conditioner for tasks such as filtering and gain adjustment, enhancing signal quality and accuracy. Subsequently, the processed vibration signals are converted to digital signals by an acquisition card and transmitted to an industrial control computer (IPC). The acquisition card typically features high-speed sampling rates, accuracy, and stability to ensure data accuracy and reliability. Finally, software programs on the IPC analyze and process the collected data.

B. Vibration Signal Acquisition

There exists a correlation between the vibration signals and the structure and operating conditions of the transformer. DC bias typically results in an uneven distribution of the magnetic field in the transformer core, leading to increased core vibration. Based on the results of the mechanical analysis of the transformer, it is observed that the

deformation of the iron core is more pronounced in the vertical direction, with noticeable deformation also observed on the top surface of the transformer shell. Therefore, in Fig. 8, arrows indicate several test points for measurement and analysis. It is imperative to place sensors at these five measurement points in the test process, ensuring that the sensors are tightly affixed to the measured surface with no gap between them. This is essential for obtaining accurate measurement results.

The initial step of the test involves measuring the vibration signal under normal conditions through a no-load test. Subsequently, varying DC currents are applied to the neutral point of the transformer for testing purposes. The vibration levels at five points are measured under normal operating conditions and with a 2 A DC bias. The vibration signals and corresponding spectra are illustrated in Fig. 9 respectively.

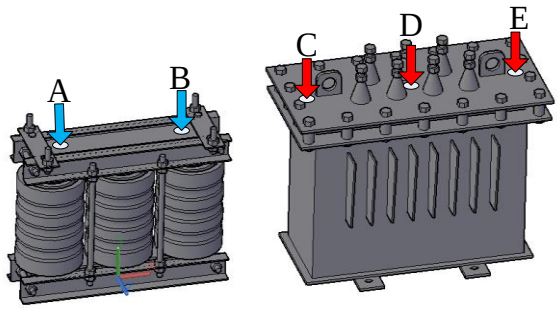

Fig.8. Vibration test point distribution

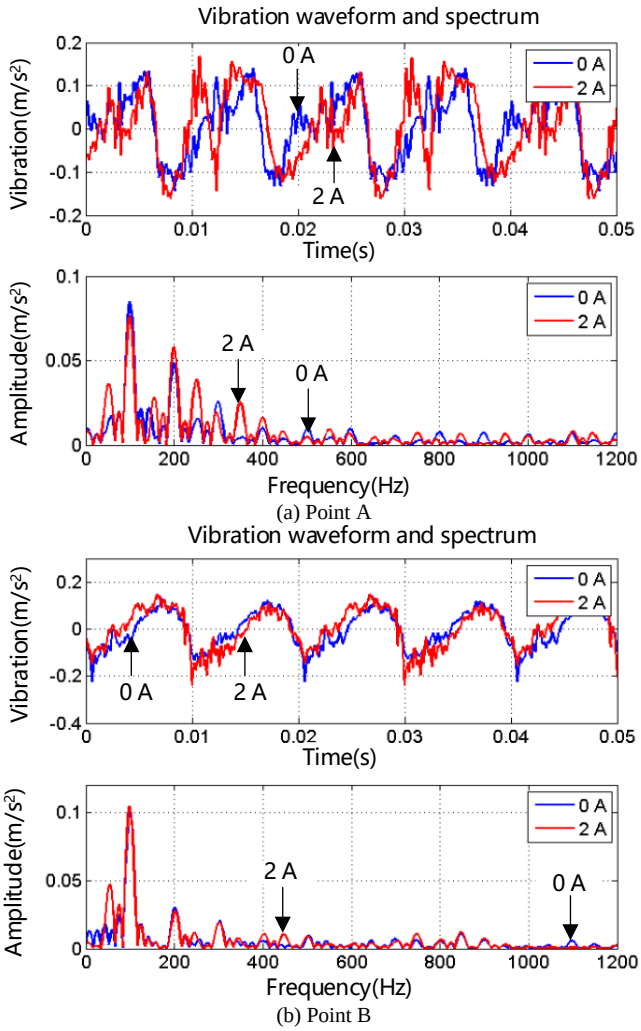

(a) Point A

(b) Point B

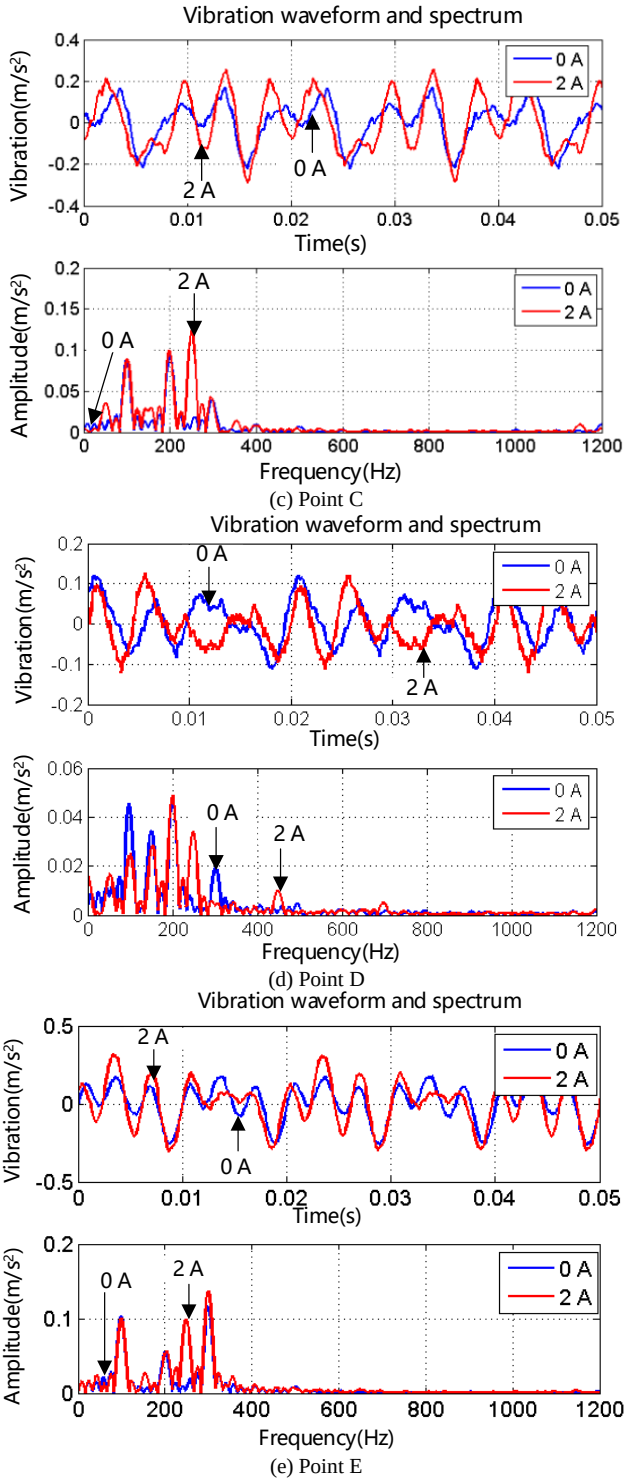

(c) Point C

(d) Point D

(e) Point E

Fig.9. Vibration measurements at each test point during transformer operation

According to the measurement results, the vibration acceleration signals at different points of the transformer mainly contain components of 50 Hz frequency and its octave. The vibration acceleration waveform changes significantly at each test point when 2 A DC is added to the neutral point of the transformer. In the vibration signals of points A and B of the iron core, the components of the 50 Hz frequency and its multiples (100 Hz, 150 Hz, etc.) increase significantly; the vibration signals of points A and B can intuitively reflect the frequency of the iron core and Vibration of the structural parts. From the perspective of the vibration signal characteristics, the vibration component at point A is richer than that at point B. For the vibration signals at the top of the transformer at points C, D, and E,

the 250 Hz component is significantly increased. The 50 Hz component of the vibration at the top point C also increases, while the 100 Hz component of the vibration at the top center point decays quickly. When DC bias is present in a transformer, the vibration will contain other odd harmonics such as 50 Hz, 150 Hz, 250 Hz, etc. However, high frequencies above 800 Hz will change irregularly with increasing DC bias and can be considered as a result of the mixing of vibration signals and noise.

C. Vibration Characteristics under DC Bias

To investigate the harmonic variations of transformer vibration under the influence of DC bias, a DC ranging from 0 to 2 A is applied to the transformer, and its vibration signal is measured. The optimized signal is obtained by CEEMD filtering, and the specific results are depicted in Fig. 10 In this figure, the horizontal axis represents the DC level, while the vertical axis represents the ratio of harmonic amplitude between the DC bias condition and the normal state.

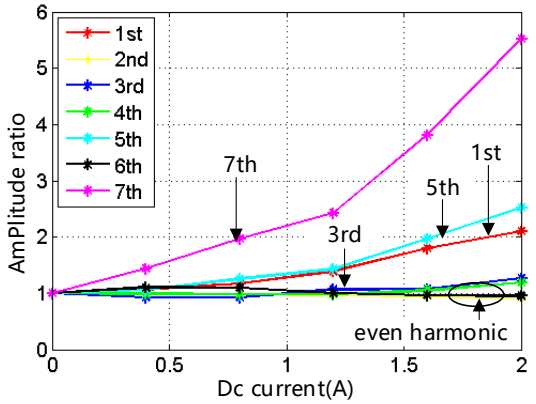

(a) Point A

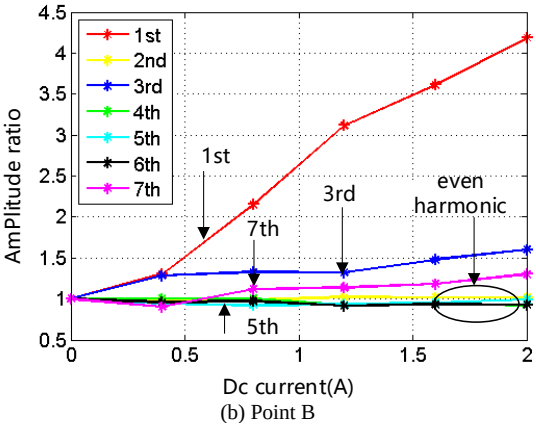

(b) Point B

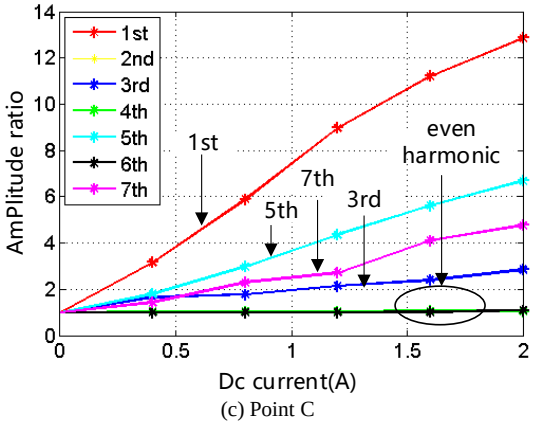

(c) Point C

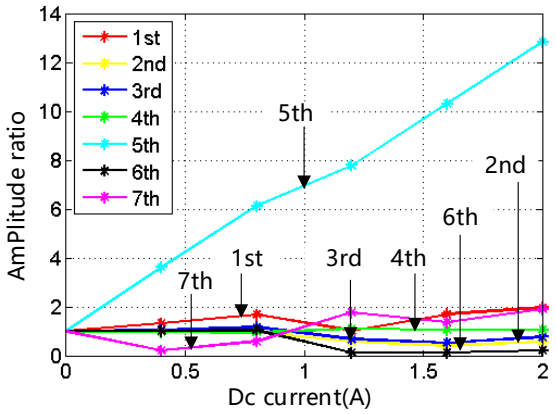

(d) Point D

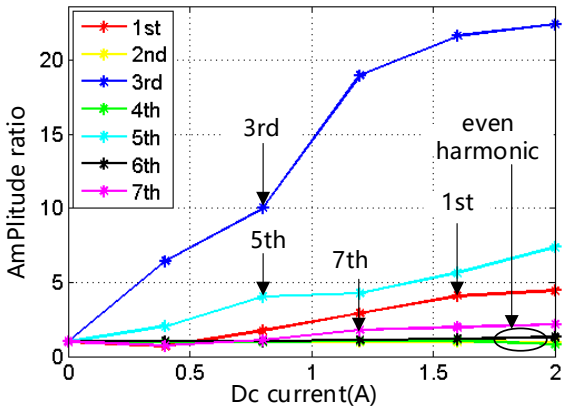

(e) Point E

Fig. 10. Transformer vibration signal harmonic ratio of each test point

Figures 10(a) and 10(b) illustrate the vibration harmonic ratios at points A and B above the transformer core. Figure 10(a) demonstrates that the odd harmonic amplitudes of core vibration increase with the DC level. The 7th harmonic (350 Hz) exhibits the most significant increase, reaching a factor of 5 when the DC reaches 2 A, whereas the even harmonics remain nearly constant. Figure 10(b) illustrates the growth of odd harmonics of the vibration signal at point B as the DC increases, with the most substantial growth in the fundamental harmonic. This phenomenon occurs due to the asymmetrical vibration between the left and right phases of the transformer, where the left side (point A) exhibits more complex vibrations than the right side (point B). Figure 10(c) displays the harmonic amplitude ratios of shell vibration, with odd harmonics increasing significantly while even harmonics remain nearly constant. The 1st harmonic (50 Hz) component increases by a factor of 13. Figure 10(d) illustrates that the 5th harmonic grows with increasing direct current, demonstrating a clear linear relationship with the DC, while the remaining harmonic components exhibit slight fluctuations from the original level. Figure 10(e) demonstrates that all harmonics of the vibration signal increase linearly with the rise in DC, while the even harmonics remain unchanged. The 3rd harmonic (150 Hz) component increases by a factor of 23. The measurements indicate that the silicon steel enters the saturation zone under the influence of the DC. Furthermore, an obvious nonlinear relationship exists between flux density and magnetostriction in the saturation region. Consequently, odd harmonics appear and increase significantly with the DC.

II. Signal Reconstruction and Analysis

A. Complementary Ensemble Empirical Mode Decomposition

Transformer vibration signals typically encompass multiple frequency components and amplitudes that vary continuously, with high-frequency signals (i.e., noise components) often failing to reflect the operational conditions of the transformer. The Complete Ensemble Empirical Mode Decomposition with Adaptive Noise (CEEMD) method effectively addresses this issue by decomposing the signal into a series of Intrinsic Mode Functions (IMFs), thereby allowing for the extraction of localized features within the signal. The CEEMD algorithm enhances decomposition efficiency by introducing both positive and negative auxiliary white noise to the original signal. This addition aids in effectively canceling out noise during ensemble averaging, thereby improving the decomposition process. The algorithm addresses challenges associated with EMD, such as substantial reconstruction errors and incomplete decomposition. [23].

Adding positive and negative Gaussian white noise to the original noise, as in Eq(1). and Eq(2):

$$s_{i1}(t) = s(t) + G(t) \tag{1}$$

$$s_{i1}(t) = s(t) + G(t) \tag{2}$$

In this equation, $S_{i1}(t)$ and $S_{i2}(t)$ is the signal after adding positive and negative noise, $s(t)$ is the original signal, and $G(t)$ is the white noise signal.

CEEMD decomposes the added positive and negative signals to obtain a series of independent IMFs. Repeat the above steps to obtain the corresponding IMF components and calculate the average of all IMF components as shown in Eq(3):

$$IMF_i = \frac{1}{sn}\sum_{i=1}^{n}\left(IMF_{i1} + IMF_{i2}\right) \tag{3}$$

In this equation, IMF_{i1} and IMF_{i2} are the IMF components with positive and negative noise decomposition added, and IMF_i is the average of the IMF components.

The signal obtained from CEEMD decomposition is shown in Eq(4):

$$S(t) = \sum_{j=1}^{N} IMF_i + R_n(t) \tag{4}$$

In this equation, $R_n(t)$ is the residual term and $S(t)$ is the decomposed original signal.

B. CEEMD-VEA-Based Transformer DC Bias Vibration Signal Reconstruction

When a DC bias is present in a transformer, the vibration will contain other odd harmonics such as 50 Hz, 150 Hz, 250 Hz, etc. However, higher frequencies above 800 Hz exhibit irregular changes with increasing DC bias, potentially due to a mixture of vibration signals and noise. Despite the CEEMD decomposition of the signal, some interference persists. Even minor interference components can significantly impact signal complexity To mitigate this effect, this paper proposes reconstructing the signal using the CEEMD-VAE method to obtain a feature signal with enhanced information accuracy. The DC bias signal at test point A is decomposed using CEEMD, as shown in Fig. 11.

Fig. 11 illustrates that the application of Complete Ensemble Empirical Mode Decomposition (CEEMD) to the vibration signal results in the formation of seven Intrinsic Mode Functions (IMFs) and one residual function. The amplitudes of IMF1 and IMF2 are notably small, approximately on the order of 10e-3. IMF1 primarily ranges between 1000 Hz and 5000 Hz, while IMF2 spans approximately 1000 Hz to 2000 Hz. These results suggest the presence of interference or noise. IMFs 3 through 7 represent the intrinsic modes of the vibration signal. CEEMD filters the signal to obtain intrinsic modes ranging from high to low frequencies. IMFs 3 to 5 display amplitudes of mid-frequency components, which are the main components of the signal. In contrast, IMF6 and IMF7 indicate that low-frequency modes are minimal. Consequently, it is important to analyze each vibration mode based on the performance of the IMFs. The frequency of transformer vibrations is predominantly concentrated below 1000 Hz.

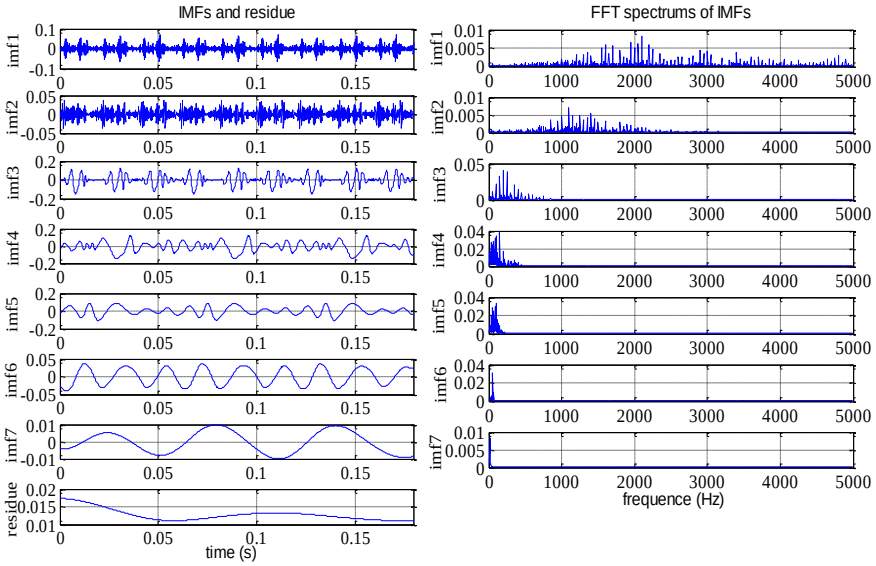

Fig.11. Vibration decompositions of A test point with DC bias by CEEMD

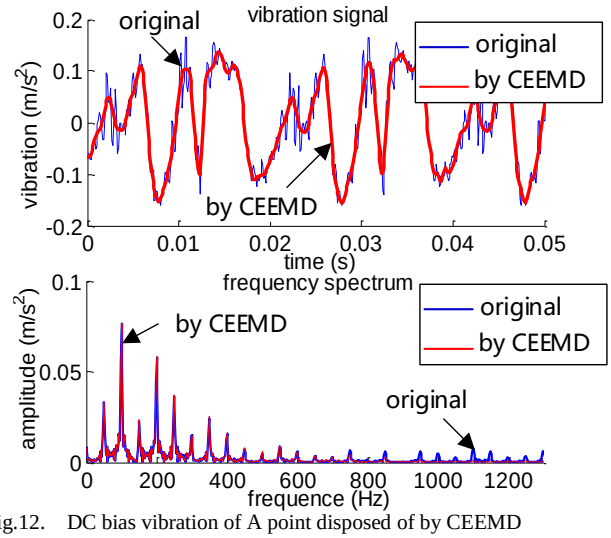

Fig.12. DC bias vibration of A point disposed of by CEEMD

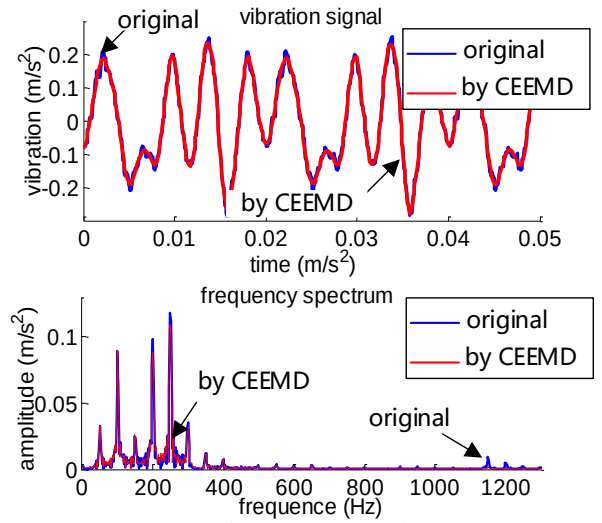

Fig.13. DC bias vibration of C point disposed of by CEEMD

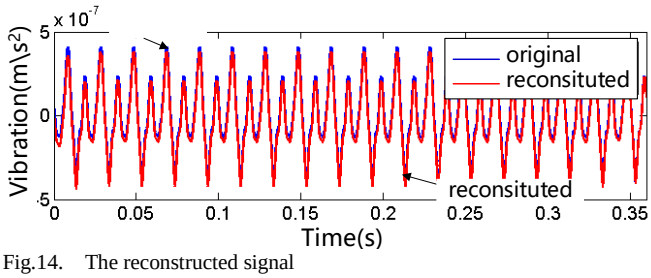

Fig.14. The reconstructed signal

IMF1 and IMF2 were filtered using CEEMD, and the results are shown in Fig. 12 and Fig. 13 This figure displays the DC bias vibration signal at test point A and point C. After filtering the first two IMFs, the signal quality is notably improved. As observed from the spectrum, frequencies above 1000 Hz are attenuated through CEEMD filtering. Similar processing is applied to signals from other test points. Each IMF component serves as input data and is reconstructed using a Variational Autoencoder (VAE). Taking point A as an example, the final reconstructed signal is depicted in Fig. 14 This approach differs from conventional low-pass filtering methods, which can only address specific frequencies rather than vibration modes. CEEMD-VAE, however, effectively identifies both noise frequencies and vibration modes, making it a robust method for processing vibration signals.

A. Characterization of Vibration Signals DC Bias

The magnetostrictive effect is crucial in analyzing the saturation characteristics of a transformer core. As the core approaches or reaches saturation, the alignment of most magnetic domains with the magnetic field direction leads to the stabilization of the magnetostrictive effect. The magnetostriction curve is depicted in Fig. 15 [24]. As the magnetic induction rises from zero to its peak and then declines back to zero, the strain curve delineates a closed region. Examination of the magnetostrictive transient waveform, illustrated in Fig. 16 [24], reveals that the strain deviates from a sinusoidal form during a cycle. This phenomenon occurs because when DC bias is present, the magnetic flux increases due to the DC, leading to asymmetry between the positive and negative half-cycles of the magnetostrictive butterfly curve, and consequently, differences in transient waveforms during each half-cycle.

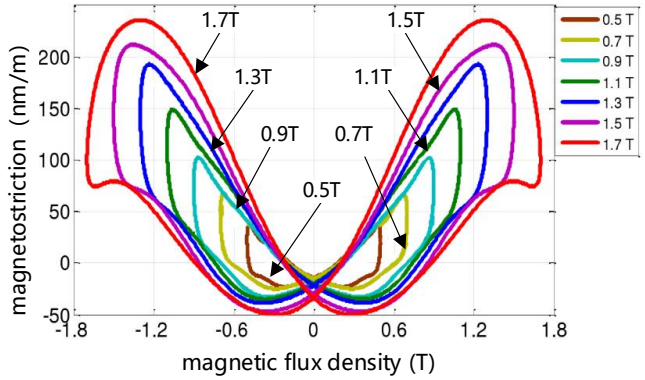

Fig.15. Butterfly curve of magnetostriction

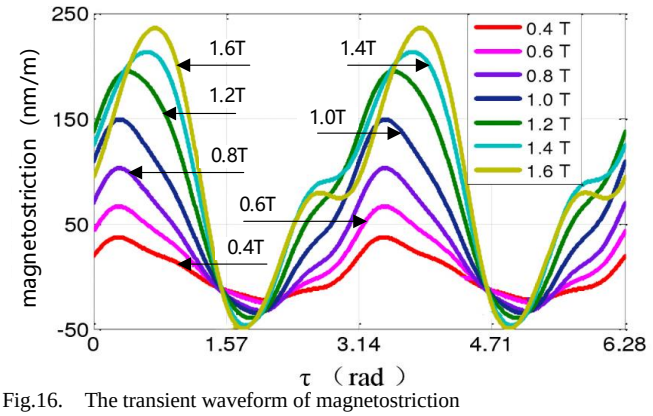

Fig.16. The transient waveform of magnetostriction

Based on this characteristic, the half-wave signal energy ratio serves as a metric for quantifying the degree of DC bias, calculated as follows Eq(5). and Eq(6):

$$\begin{cases} E_{sat} = \int_{t_0}^{t_0+\frac{T}{2}} x(t)^2 \, \mathrm{d}t \\ E_{unsat} = \int_{t_0+\frac{T}{2}}^{t_0+T} x(t)^2 \, \mathrm{d}t \end{cases} \tag{5}$$

$$F = \left(\frac{E_{sat}}{E_{unsat}} \right)_{\max} \tag{6}$$

The time-domain half-wave energy ratios of the displacement signal for both the transformer core and shell vibration, as influenced by increasing DC, have been calculated, with the results presented in Table III.

TABLE III
THE CALCULATION RESULTS OF HALF WAVE ENERGY RATE

DC(A)	A	B	C	E
0	1.315	1.445	1.120	1.169
0.2	1.329	1.454	1.125	1.214
0.4	1.316	1.472	1.177	1.232
0.6	1.367	1.741	1.211	1.592
0.8	1.428	1.922	1.277	1.913
1	1.443	2.147	1.445	2.060
1.2	1.453	2.263	1.535	2.216
1.4	1.590	2.534	1.615	2.451
1.6	1.734	2.804	1.669	2.697
1.8	1.995	3.006	1.714	2.781
2	2.319	3.183	1.762	2.877

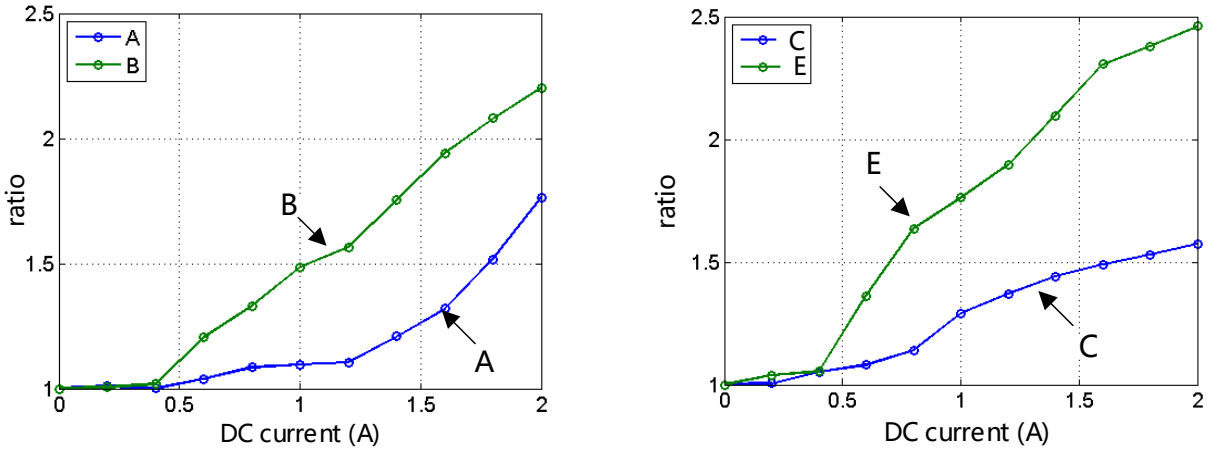

(a) Point A and Point B (b) Point C and Point E

Fig.17. Analysis of the half wave energy rate of vibration signals in normalization

The results in Table III indicate that the half-wave energy ratios of vibration at the test points on both the core and the transformer shell increase with rising DC. To further ascertain the impact of factor F on DC bias, the normalized half-wave energy ratio is derived by comparing the calculated results under various DC currents with those obtained under unbiased conditions, as illustrated in Fig. 17.

In summary, the analysis reveals a positive correlation between the calculated results for the iron core (points A and B) and the top of the transformer shell (points E and F) and the magnitude of DC bias. As the DC increases, F also rises, suggesting that under cyclic alternating current, the core material experiences greater magnetostrictive differences between the first and second half-cycles, thereby creating a significant disparity in signal energies between cycle halves. Therefore, from the above analysis, it can be inferred that the half-wave energy ratio of the calculated signal effectively quantifies the degree of transformer DC bias.

A. Fuzzy Entropy

Fuzzy entropy represents a sophisticated method for quantifying the complexity of time series data. It employs an exponential function for fuzzification, thereby ensuring stable and continuous variations in fuzzy entropy. Moreover, the application of a mean value operation effectively mitigates the adverse effects of baseline drift on entropy values. The computation of fuzzy entropy generally involves the evaluation of the affiliation function of elements within a set. The affiliation function quantifies the extent to which each element is associated with the fuzzy set. Higher values of the affiliation function denote a greater degree of relevance, while lower values signify reduced relevance. [25], [26].

Phase space reconstruction of a set of time series X of length N yields a time series Y as shown in Eq(7):

$$Y(i)=\begin{bmatrix} x(i), x(i+1),\ldots, \\ x(i+m-1) \end{bmatrix}-x_0(i), i = 1,2,\ldots,N-m+1 \tag{7}$$

In this equation, m is the mode dimension and $x_0(i)=\frac{1}{m}\sum_{j=0}^{m-1}x(i+j)$ is the mean value.

Define the distance between two-time series $Y(i)$ and $Y(j)$ as shown in Eq(8):

$$d_{i,j}^{m}=d\left[Y(i),Y(j)\right] = \max_{k\in(0,m-1)}\left|\begin{matrix}\left(x(i+k)-x_0(i)\right)- \\ \left(x(j+k)-x_0(j)\right)\end{matrix}\right| \tag{8}$$

The fuzzy affiliation function is introduced, and the fuzzy function is utilized to calculate the similarity between the time series $Y(i)$ and $Y(j)$ as shown in Eq(9):

$$D_{i,j}^{m}=\exp\left[-\frac{\left(d_{i,j}^{m}\right)^{n}}{r}\right] \quad (9)$$

In this equation, r is the similarity tolerance limit, $i,j=1,2,\ldots,N-m+1$, and $i\neq j$.

The defining function is shown in Eq(10):

$$\Phi^{m}(i)=\frac{1}{N-m+1}\sum_{i=1}^{N-m+1}\left(\frac{1}{N-m}\sum_{j=1,j\neq i}^{N-m+1}D_{i,j}^{m}\right) \quad (10)$$

The fuzzy entropy of the original time series is shown in Eq(11):

$$FuzzyEn(m,r)=\lim_{N\to\infty}\left[\ln\Phi^{m}(r)-\ln\Phi^{m+1}(r)\right] \quad (11)$$

For a finite length time series, the fuzzy entropy is estimated as shown in Eq(12):

$$FuzzyEn(m,r,N)=\ln\Phi^{m}(r)-\ln\Phi^{m+1}(r) \quad (12)$$

B. Fuzzy Entropy of Vibration Signals under DC Bias Magnetization

Vibration signals were monitored at five different locations, namely A, B, C, D, and E, situated at the top of the core and enclosure, as depicted in Fig. 8. Various DC currents were injected into the neutral point of the transformer, and the corresponding vibration waveforms were measured. To mitigate the impact of system noise present in the experiments, the five sets of measurements underwent CEEMD-VAE filtering. In this study, FuzzyEn was calculated using established parameter values of m = 2 and r = 0.2 std (x) across DC currents ranging from 0 to 3.2 A. The FuzzyEn calculations for the five sets of results are presented in Table IV.

The data in Table IV indicate that the FuzzyEn values for all groups are less than 1. Groups A and B exhibit significantly higher values compared to Groups C, D, and E. This consistency across all groups suggests a common trend. The attenuation of high-frequency components during transmission from the core to the shell may contribute to this phenomenon. Additionally, Fig. 12 and Fig. 13 reveal that the waveforms of core vibration are more complex than those of shell vibration. This observation suggests that FuzzyEn accurately reflects the chaotic nature of the vibration signal.

TABLE IV
FUZZYEN OF VIBRATION SIGNALS

DC(A)	A	B	C	D	E
0	0.8428	0.7264	0.459	0.6683	0.6027
0.4	0.886	0.8144	0.5315	0.7231	0.6825
0.8	0.9069	0.8323	0.5515	0.7493	0.6813
1.2	0.9252	0.8473	0.5718	0.8259	0.7274
1.6	0.9408	0.8229	0.5419	0.7967	0.6968
2	0.9232	0.8295	0.5301	0.8229	0.692
2.4	0.9032	0.8095	0.5001	0.8029	0.652
2.8	0.8532	0.7695	0.4301	0.7429	0.602
3.2	0.8032	0.7295	0.4294	0.7029	0.592

C. Fuzzy Entropy Curve Analysis

A cubic spline interpolation function is used to fit the FuzzyEn values and derive the variation rule of the FuzzyEn value under DC bias, and the results are shown in Fig. 18.

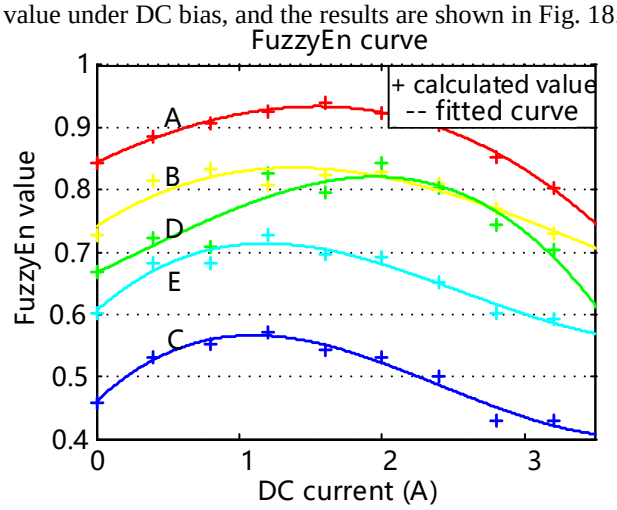

Fig.18. FuzzyEn change with DC

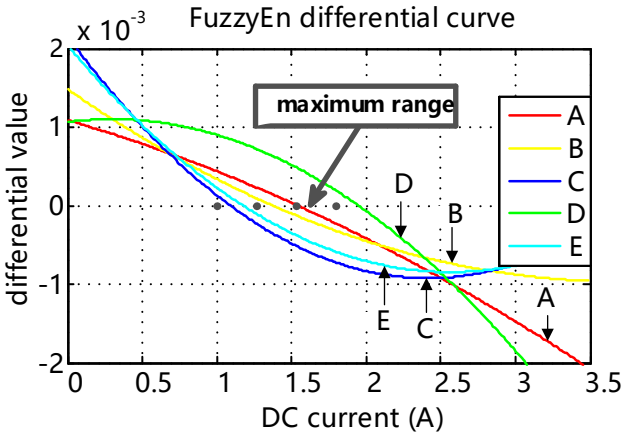

Fig.19. FuzzyEn Differential Curve with DC Current

It is observed that all five FuzzyEn curves exhibit an initial increase followed by a decrease as the DC bias intensifies. Fig. 19 illustrates the differential curves of each FuzzyEn along with the range of extreme values for the five curves. The results indicate that the maximum FuzzyEn value occurs at approximately 1.5 A on the left and right sides of the core (Groups A and B); on the left and right sides of the housing (Groups C and E), the maximum value is around 1 A. In the middle of the housing (Group D), the maximum FuzzyEn value is approximately 2 A.

When the signal comprises solely the fundamental frequency, the FuzzyEn value is typically low, indicating minimal signal complexity. As DC bias intensifies, it influences the vibration signal, leading to a gradual increase in odd harmonics. During this phase, the fundamental frequency persists as the dominant component, while harmonics serve as secondary elements. Consequently, the FuzzyEn value rises, signifying increased signal complexity. The core reaches saturation when the FuzzyEn value of the vibration signal attains its peak. Subsequently, as odd harmonics surpass the fundamental frequency, the signal's main components transition to harmonics, resulting in decreased signal complexity. At this point, the FuzzyEn value decreases. The DC bias condition of the transformer core can be evaluated by monitoring changes in the FuzzyEn

value. Real-time monitoring of transformer vibrations using the FuzzyEn value facilitates the analysis of the DC bias condition and determination of the iron core's saturation state. Additionally, by analyzing the FuzzyEn value and the differential curve under DC bias, it can be concluded that the iron core is in a saturation state when the differential curve is positioned above the zero threshold.

The observed phenomenon can be elucidated through the concept of magnetostriction in the iron core. When DC flows into the neutral point, the magnetic flux within the core intensifies to the extent that it enters the saturation region. The pronounced nonlinearity of magnetostriction exacerbates this effect, increasing vibration harmonics. As per the obtained results, it's evident that under DC bias, odd harmonics experience significant enhancement while even harmonics remain largely unaffected. Additionally, FuzzyEn serves to evaluate the complexity of the signal, enriching the sequence composition of the harmonics. The FuzzyEn increases until the DC reaches approximately 1 A, after which it remains relatively unaffected by further changes in DC. However, as the DC bias exceeds approximately 2 A, odd harmonics become the dominant components of the signal, leading to a decrease in the even harmonics. Consequently, the complexity of the signal decreases with the increase in odd harmonics. In conclusion, the variation in FuzzyEn allows for the analysis of the DC bias condition of the transformer core. The differential curve saturates in the region where the iron core transitions past zero, providing insight into the core's saturation state.

III. Conclusion

In this paper, CEEMD (Complementary Ensemble Empirical Mode Decomposition) is utilized to process vibration signals from transformers. CEEMD adaptively decomposes these signals into Intrinsic Mode Functions (IMFs), which are then reconstructed using a Variational Autoencoder (VAE). This approach aims to enhance the clarity of vibration signals by selectively removing noise and isolating specific frequency components.

A sophisticated vibration testing system is employed to monitor five strategic points on the transformer core and its casing. Through the application of CEEMD decomposition and subsequent reconstruction, researchers conduct a comparative analysis of vibration patterns under standard operational conditions and during DC bias. The study reveals that DC bias significantly alters the vibration characteristics of the transformer core and casing, particularly by nonlinearly increasing odd harmonics while keeping even harmonics relatively stable across varying DC levels. Another crucial element of the study is the employment of FuzzyEn (Fuzzy Entropy) as a method for assessing the onset of DC bias in transformers. By examining the vibrations at these five testing points, researchers demonstrate that changes in FuzzyEn values and their differential curves accurately reflect the degree of core saturation caused by DC bias. The findings of this research emphasize that the iron core transitions into a saturation region when the FuzzyEn value of the vibration signal reaches its maximum, and the differential curve saturates beyond the zero thresholds.

Ultimately, real-time monitoring of transformer vibrations, integrated with FuzzyEn analysis, has proven to be an effective approach for assessing DC bias conditions and determining the saturation state of the iron core. This capability is essential for ensuring the reliability of power grid operations, particularly in situations where severe DC bias may occur, requiring prompt corrective actions.

References

[1] G. l. Zhao, G. Y. Qiao, Z. Y. Yu, T. Chen, and Y. Wang, “A Review of Research on Transformer DC Bias Caused by HVDC Transmission,” Journal of Physics: Conference Series, vol. 2310, no. 1, pp. 12-27, 2022.

[2] X. Y. Zhang, C. Chao, P. H. Mo, Q. G. Gu, and Z. M. Sun, “Influence of DC Magnetic Bias on Transformer Protection and Improvement of DC Magnetic Bias Protection,” Automation of Electric Power Systems, vol. 45, no. 4, pp. 148-154, 2021.

[3] C. Pan, S. Y. Yi, H. Su, and W. X. Shi, “Excitation–vibration harmonic response research of transformer in DC biasing operation,” IET Electric Power Applications, vol. 13, no. 3, pp. 410-417, 2019.

[4] B. Li, Z. Z. Wang, M. Y. Li, and S. X.Guo, “Analysis of the DC Bias Effects on the UHV Autotransformer with Rated Load Based on a Reduced-Scale Model Experiment,” Applied Sciences, vol. 10, no. 4, pp. 1529-1542, 2020.

[5] Y. Q. Wang, L. Li, X. J. Zhao, and J. Sun, “Analysis of DC bias characteristics of the transformer by using fixed-point time-step FEM and dynamic J–A hysteresis model,” AIP Advances, vol. 14, no. 3, 2024.

[6] X, Y, Jia. B. Wang, M. Lin, J. Yang, and Q. W. Wang, “Electromagnetic and Thermal Characteristics Simulation for Three-phase Three-limb Transformers under DC magnetic bias,” Heat Transfer Research, vol. 54, no. 12, pp. 39-59, 2023.

[7] Mikhak-Beyranvand. M, Faiz. J, Rezaeealam. B, “Thermal analysis and derating of a power transformer with harmonic loads,” IET Generation, Transmission Distribution, vol. 14, no. 7, pp. 1233-1241, 2020.

[8] Z. W. Chen, Q. P. Zhou, G. C. Ding, X. W. Wu, J. Wu, and Y. J. Zhang, “Influence of Magnetic State Variation on Transformer Core Vibration Characteristics and Its Measurement,” IEEE Transactions on Instrumentation and Measurement, vol. 71, no. 1, pp. 1-13, 2022.

[9] Z. Wang, Z. M. Fan, X. Li, K. Xu, and R. J. Yu, “Measurement of Magnetic and Magnetostrictive Characteristics of Transformer Core Based on Triaxial Strain Gauge and B-H Vector Sensor,” Sensors (Basel, Switzerland), vol. 23, no. 13, pp. 5926-5941, 2023.

[10] X. L. Yan, D. Xia, G. Z. Han, X. D. Yu, and F. Y. Ma, “Research on the Magnetostrictive Characteristics of Transformers under DC Bias,” Energies, vol. 16, no. 11, pp. 4457-4472, 2023.

[11] D. Z. Chen, B. Q. Hou, Z. Y. Feng, and B. D. Bai, “Study of Magnetostriction Influence of Electrical Sheet Steel Under Different DC Biases,” IEEE Transactions on Magnetics, vol. 55, no. 2, pp. 1-5, 2019.

[12] Y. Sun, Z. H. Wu, Y. S. Zhang, and L. Weng, “Analysis of the influence of permanent magnet on the torsional strain of waveguide wire of the magnetostrictive displacement sensor,” Chinese Journal of Scientific Instrument, no. 4, pp.10-23, 2021.

[13] W. Guo, X, M, Liu, Y. Ma, Y. M. Yang, and Annad. Jado, “Bias magnetic characteristic analysis and condition identification of transformers under DC bias magnetism conditions based on electromagnetic vibration and convolutional neural network,” vol. 557, pp. 169470-169485, 2022.

[14] S. E. Zirka, Y. I. Moroz, J. Elovaara, M. Lahtinen, R. A. Walling, H. Kr. Høidalen, D. Bormann, C. M. Arturi, and N. Chiesa, “Simplified models of three-phase, five-limb transformer for studying GIC effects,” International Journal of Electrical Power and Energy Systems, vol. 103, pp. 168-175, 2018.

[15] J. Liu, W. Niu, L. Zhao, Z. K. Tan, and H. R. Zeng, “State identification method for transformer of urban power grid under DC bias based on vibration signal,” Journal of Electric Power Science and Technology, vol. 36, no. 5, pp. 169-178, 2021.

[16] M. M. Ai, W, H, Liu, and Y. Shan, “Research on power transformer vibration and noise under DC bias condition,” International Journal of Applied Electromagnetics and Mechanics, vol. 68, no. 3, pp. 371-385,2022.

[17] H. B. Ding, W. L. Zhao, M. Li, L. Zhang, and Y. L. Sun, “Electromagnetic Vibration Characteristics of High-Frequency

Transformer under DC Bias with Different Winding Structures," Processes, vol. 11, no. 4, 2023.
[18] C. Y. Li, N. C. Zhou, J. Q. Liao, and Q, G, Wang, "Multiscale multivariate fuzzy entropy-based technique to distinguish transformer magnetizing from fault currents," IET Generation, Transmission Distribution. Vol. 13, no. 12, pp. 2319-2327, 2019.
[19] J. Li, C. Liu, Z. F. Zeng, and L. N. Chen, "GPR Signal Denoising and Target Extraction With the CEEMD Method," IEEE Geosci. Remote Sensing Lett, vol. 12, no. 8, pp. 1615-1619, 2015.
[20] M. N. L. Anuradha, C. H. Vasavi, T. Srinivasa. Rao, and G. Suresh. Kumar, "Fuzzy Integro Dynamic Equations on Time Scales using Fuzzy Laplace Transform Method," Engineering Letters, vol. 31, no. 3, pp. 1114-1121, 2023.
[21] Junhong Chen, Hong Dai, Shuang Wang, and Chengrui Liu, "Improving Accuracy and Efficiency in Time Series Forecasting with an Optimized Transformer Model," Engineering Letters, vol. 32, no. 1, pp. 1-11, 2024.
[22] X. Y. Zhang, X. H. Liu, F. H. Guo, G. X. Xiao, and P. Wang, "Calculation of DC Bias Reactive Power Loss of Converter Transformer via Finite Element Analysis," IEEE Transactions on Power Delivery, no. 99, pp. 1-1, 2020.
[23] T. X. Han, Y. H. Shi, M. W. Li, J. Y. Liang, and Y. R. Yang, "Study on the prediction of heated area ash fused with CEEMD and TCN," Journal of Electronic Measurement and Instrumentation, vol. 36, no. 10, pp. 108-114, 2022.
[24] H. L. Liu, "Multi-physics field coupling problem of transformer core vibration noise," Shenyang University of Technology, 2014.
[25] A. M. S. Borin, L. E. V. Silva, L. O. Murta, "Modified multiscale fuzzy entropy: A robust method for short-term physiologic signals," Chaos An Interdisciplinary Journal of Nonlinear Science, vol. 30, no. 8, pp. 083135-083144, 2020.
[26] Y. T. Wang, D. Wang, "Investigations on sample entropy and fuzzy entropy for machine condition monitoring: revisited," Measurement Science and Technology, vol. 34, no. 12, pp. 107497-107510, 2023.